scientific reports

OPEN

Three-dimensional thermomechanical modelling beneath Guerrero, Mexico, and its relation to the occurrence of interplate seismic phenomena

Nobuaki Suenaga[1]✉, Shoichi Yoshioka[1,2], Vlad Constantin Manea[3], Marina Manea[3], Erika Jessenia Moreno[1] & Yingfeng Ji[4,5]

In this study, we investigated the relationships among the occurrence regions of megathrust earthquakes and slow earthquakes, estimated interplate temperatures, and dehydration processes at the plate interface in the subduction zone of the Cocos plate in Mexico, with a focus on the Guerrero seismic gap. For this purpose, we performed a series of 3-D thermomechanical numerical simulations of subduction based on a combination of multiple unknown model parameters. Comparing the temperature field for the optimal model with the occurrence region of the interplate seismic phenomena, the temperature along the slab surface where megathrust earthquakes tend to occur is estimated to range from 200 to 400 °C. In addition, the occurrence areas of recent long-term slow slip events (hereafter referred to as L-SSEs) with a recurrence interval of ~ 4 years in the range where the amount of slip is 10 cm or more correspond to a temperature range of 350 to 550 °C outside the Guerrero seismic gap region. On the other hand, in the Guerrero seismic gap region, L-SSE slip is observed up to shallower areas, but the updip limit temperature in the region with the largest slip amount (~ 14 cm) is also estimated to be approximately 350 °C. Furthermore, for regions affected by tectonic tremors (hereafter referred to as TTs) within seaside swarms and inland swarms, our temperature estimates range from 500 to 570 °C and from 600 to 700 °C, respectively. Finally, we compared the estimated dehydration processes on the plate interface for the optimal model with interseismic events. These findings suggest that considerable dehydration from MORB within the oceanic crust and ultramafic rock within the slab mantle occurred near long-term slow slip events and tectonic tremor regions.

On the Pacific side of Mexico, the Cocos plate is currently subducting beneath the North American plate along the Middle America Trench (MAT) at a convergence rate of approximately 6.6 cm/yr in the north-northeast direction[1]. In this region, M8-class megathrust earthquakes such as the 1985 Michoacan earthquake (Mw8.0), the 1995 Colima-Jalisco earthquake (Mw8.0), and the 2017 intraslab Tehuantepec earthquake (Mw8.2) have occurred. Additionally, the Guerrero seismic gap has existed in coastal regions for more than 100 years (Fig. 1)[2]. In addition, interplate slow earthquake phenomena such as slow slip events (SSEs)[3] and tectonic tremors (hereafter referred to as TTs) are observed near Guerrero, southeastern Mexico[4,5]. In this region, the so-called "flat slab" exists adjacent to the 1000 km long Neogene continental arc called the Trans-Mexican Volcanic Belt (TMVB). A previous study yielded a resistivity model[6] and proposed a probable mega-intrusion rock or serpentinized mantle material located in the continental crust above the tip of the mantle wedge[5] along the across-arc profile passing through Acapulco, the area adjacent to the eastern end of the Guerrero seismic gap. This hypothesis is useful for explaining the observed gravity and magnetic anomalies around the Guerrero seismic gap.

[1]Research Center for Urban Safety and Security, Kobe University, Rokkodai-Cho 1-1, Nada Ward, Kobe 657-8501, Japan. [2]Department of Planetology, Graduate School of Science, Kobe University, Rokkodai-Cho 1-1, Nada Ward, Kobe 657-8501, Japan. [3]Computational Geodynamics Laboratory, Instituto de Geociencias, Universidad Nacional Autónoma de México, Campus Juriquilla, Querétaro 76230, México. [4]Institute of Tibetan Plateau Research, Chinese Academy of Sciences, Lincui Road 16-3, Chaoyang, Beijing 100101, China. [5]University of Chinese Academy of Sciences, Lincui Road 16-3, Chaoyang, Beijing 100101, China. ✉email: n.suenaga@people.kobe-u.ac.jp

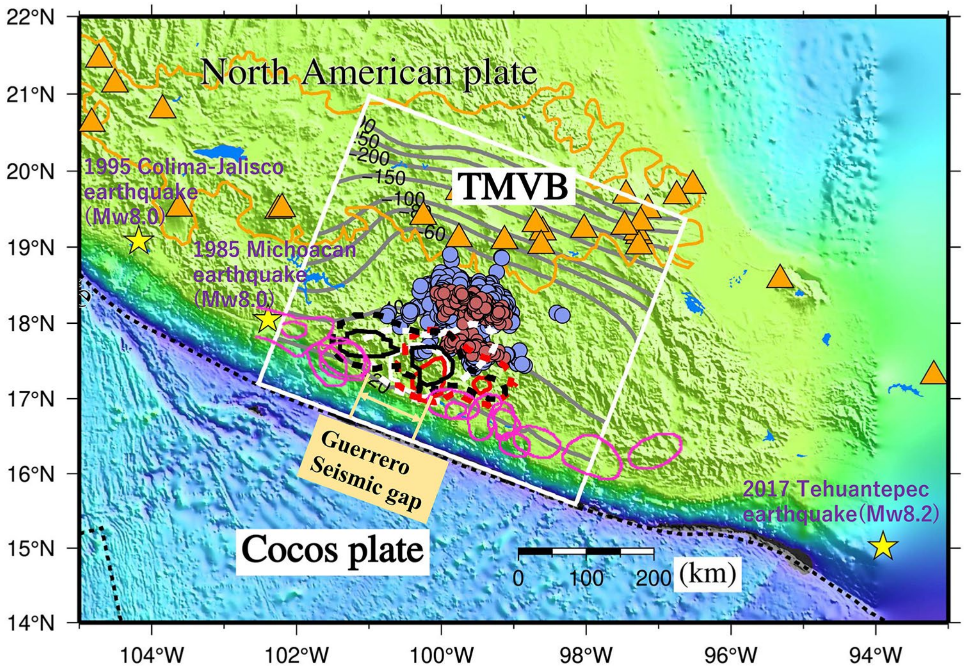

Fig. 1. Tectonic map of southern Mexico. The area surrounded by the white frame represents the model region for numerical simulation in this study, including the Guerrero seismic gap. The gray solid lines represent the isodepth contour lines of the upper surface of the subducted Cocos plate at 20-km intervals depicted in Fig. S2[16,17,43]. Yellow stars indicate the epicentres of recent M8-class megathrust earthquakes. Orange triangles and the contour line represent volcanic chains within the TMVB and its region, respectively. The pink and purple solid circles represent epicentres of tectonic tremors during the period from January 1, 2005 to June 6, 2007 observed by MASE stations and from November 26, 2009 to August 17, 2013 observed by GGAP stations, respectively (Idehara et al., 2014)[4]. The white, black, and red contour lines represent the areas where the cumulative slip amounts of the three L-SSE events in 2001–2002, 2006, and 2009–2010 are 10 cm or greater at 4 cm contour intervals, respectively[3]. For each L-SSE event, the 10 cm slip contours are plotted as dashed lines and the 14 cm slip contours are plotted as solid lines. The pink contour lines represent the rupture areas caused by past megathrust earthquakes[44]. The map was created using the Generic Mapping Tools (GMT)[41] (version 4.5.7, https://www.generic-mapping-tools.org/download/).

A previous study[7] estimated the width of the seismogenic zone of southern Mexico in the Guerrero seismic gap area by performing 2D steady-state thermal modelling. The updip limit of the seismogenic zone where smectite transforms to illite and chlorite (100 to 150 ℃) was estimated to be located 15–20 km landward of the MAT in their numerical simulation. The downdip limit of the seismogenic zone where quartzo-feldspathic rocks initiate to change their slip mode from velocity weakening to velocity strengthening (320 to 350 ℃) was estimated to be located at a horizontal distance of 90–110 km from the trench. Additionally, in these numerical simulations, a small fraction of frictional heating was necessary to fit the thermally estimated seismogenic zone with the observed rupture areas of megathrust earthquakes. The authors determined an effective frictional coefficient of 0.051 to best fit the observed heat flow data. Wada and Wang (2009)[8] performed 2D thermal modelling near northern Mexico and determined that the coupling-to-decoupling transition depth at the plate interface reached an interplate depth of approximately 40 km. Manea and Manea (2011)[9] also performed 2D thermal modelling near the Guerrero gap and suggested that the sedimentary layers dehydrate approximately three-quarters of the water content above the flat slab at a horizontal distance of approximately 300 km from the MAT and that this region corresponds to the region where TTs take place. Rosas et al. (2016)[10] performed 3-D steady-state thermal modelling to investigate flow patterns in the mantle wedge accompanied by geometric variations in the Cocos plate. They also considered hydrothermal circulation in an aquifer in the subducting oceanic crust and suggested that the effect of hydrothermal circulation reduces the interplate temperature, but mainly in the shallow region. However, 3-D time-dependent thermal modelling has not yet been performed in southern Mexico, whose thermal structure is constrained by high-density Curie point depth data[11]. The global Curie point depth distribution dataset they analysed has been published with dense data intervals of 2-min arcs, which were used in this study.

Here, we constructed a 3-D thermomechanical model for southern Mexico to elucidate the relationships among the calculated temperature structure, dehydrated water content from the subducting Cocos plate, and above-mentioned interplate seismic phenomena, with a particular focus on the region including the Guerrero seismic gap.

Model setting

Following Ji and Yoshioka (2015)[12], we constructed a preliminary 3-D thermomechanical model to calculate the temperature and flow fields associated with subduction of the Cocos plate[13] and then improved the model. The size of the model in this study is 450, 500, and 200 km in the x-, y-, and z-axis directions, respectively (Fig. 2). The number of grid points used in the model is 36 × 41 × 101, indicating grid spacings of 12.86, 12.5, and 2.0 km, respectively.

For the boundary conditions of flow fields, we applied permeable conditions whereby mantle flow that comes into contact with the boundary surface passes through it without being reflected or refracted at the boundaries of + x, -x, + y, −y, and −z, where the mantle flow comes into contact except for the Earth's surface, where three components of flow velocity are assumed to be 0. In terms of the temperature boundary conditions, a temperature of + z corresponding to the Earth's surface is given as a fixed temperature (0 ℃). At the boundary of + x, where the oceanic plate initiates subduction, we assume a plate cooling model[12] to obtain the depth- and age-dependent temperature, referring to the spatiotemporally changing seafloor age on this + x boundary for each time step in the numerical calculation. However, considering the seafloor topography, we assume that the seafloor temperature is 0 ℃, which is the same as the Earth's surface, and the equation for the plate cooling model in the preceding study[14] can be modified as follows:

$$T(z,t) = T_0 + (T_1 - T_0)\left[\frac{z-d_s}{d_l} + \frac{2}{\pi}\sum_{n=1}^{\infty}\frac{1}{n}\,exp\left(-\frac{\kappa n^2\pi^2 t}{{d_l}^2}\right)\,sin\left(\frac{n\pi z}{d_l}\right)\right] \tag{1}$$

where T_0 and T_1 are the temperatures at the model surface and the base of the lithosphere, respectively; Z is the depth; d_s is the seafloor depth at the trench axis; d_l is the depth at which the mantle temperature reaches T_1; n is an index; κ is the thermal diffusivity; and t is the age of the Cocos plate at the MAT. We used the RT1[15] model, in which the values of T_1 and d_l were 1402 ℃ and 134.9 km, respectively. Fig. S1 shows the temperature as a function of depth with and without the parameter of seafloor depth d_s in Eq. (1) for the plate cooling model.

For other temperature boundary conditions, we applied adiabatic conditions whereby there was no spatial temperature variation when passing through the boundaries of −x, + y, −y, and −z. The initial temperature condition in the model was also determined by the plate cooling model.

The geometry of the subducting Cocos plate was determined with reference to several data. First, we used ETOPO1[16] as the bathymetry data (Fig. S2a). In addition, we used a slab surface geometry focused in and around the Guerrero gap region, where negative Bouguer gravity anomalies are observed, suggesting decreased underground density (Fig. S2b)[17]. Recent studies have reported negative residual gravity within the Guerrero seismic gap sandwiched by positive residual gravity in the along-arc direction of the seismogenic zone. In the positive residual gravity region, seamounts are subducted to depth along the seismogenic zone, whereas in the negative region, the subducted seamounts are located at a shallower plate interface than in the seismogenic zone[18]. We then used the Slab 2.0 model in other regions (Fig. S2c). The final plate geometry model (Fig. S2d) used in the numerical simulation was determined by combining them. To connect the geometry data and bathymetry data,

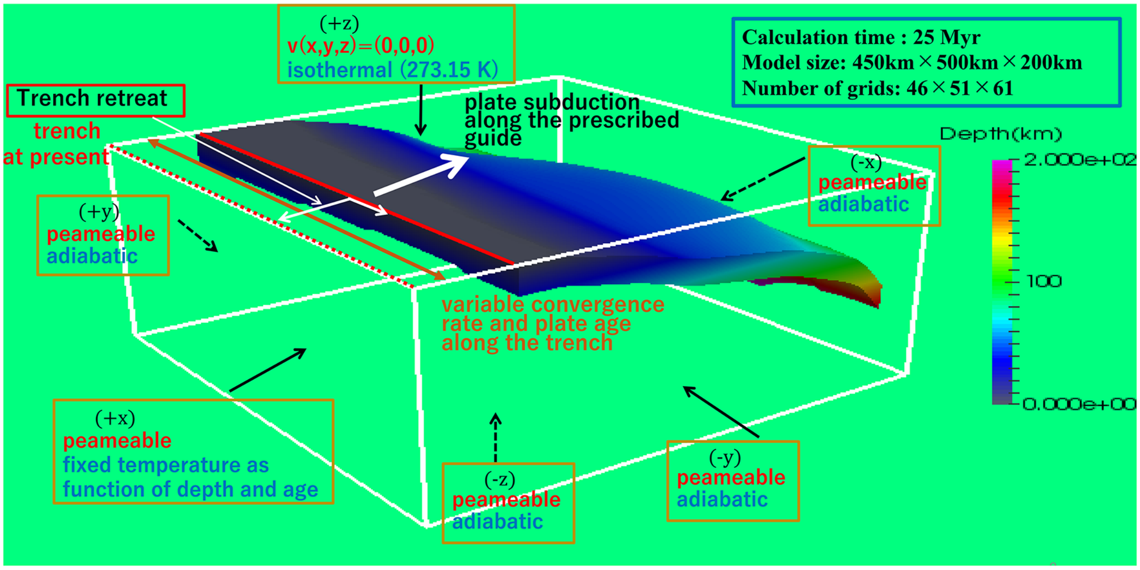

Fig. 2. Schematic of the 3-D Cartesian thermomechanical subduction model used in this study. The boundary conditions for mantle flow and the temperature field at the respective boundaries are noted with red and blue letters, respectively. This figure was created using ParaView[42] (version 5.4.1, https://www.paraview.org/download/).

we used adjustable tension continuous curvature splines with the maximum tension factor to minimize depth discontinuity at the joints between the data. Because the plate geometry is concave in and around the Guerrero seismic gap, we investigated this effect on the temperature variation and dehydration process around the plate interface in the along-arc direction.

In this study, the current subducting slab shape shown in Fig. S2d was used as a fixed slab guide within the model domain, where slab material is funnelled at a convergence rate between the Cocos plate and the North American plate to reproduce the subduction of the oceanic plate. The model consisted of the subducting oceanic plate within the prescribed guide, the upper and lower crust with respective thicknesses of 16 km, an accretionary prism, a high viscosity region within the mantle wedge, and the mantle (Fig. S3). The domains of the upper crust, lower crust, and accretionary prism were rigid, where only conductive heat transport occurred. The other domains were composed of convective regions.

Previous studies of the subduction history of the Cocos plate near the model region[19] and the global plate motion model[20–22] were used to determine the relative motion of the Cocos plate with respect to the North American plate (Table S1).

In the model region, trench retreat has been suggested by the arrangement of the Colima rift and the formation of a flat slab[19,23,24]. We also referred to a global plate motion model[25,26] that estimated the trench retreat rate using a hotspot reference frame. We set the trench retreat rate to 1.5 cm/yr from 15 to 10 Ma, 1.0 cm/yr from 10 to 5 Ma, and 0.5 cm/yr from 5 Ma to the present in our calculations (Fig. S4).

In this study, we evaluated the validity of the simulated thermal structures by comparing the calculated Curie point depth[11], which has never been used before except for by Iwamoto et al. (2023)[27], with the calculated depth to constrain our thermal structure model. The global Curie point depth model[11] is estimated as the depth of isotherms at 550 ℃, above which the magnetism loses its strength, using the Earth Magnetic Anomaly Grid (EMAG2)[28]. The global Curie point depth distribution dataset that they analysed has been published, and we used this dataset. In this study, we changed multiple parameter values within a certain range and performed several numerical calculations. The optimal model was then selected with a minimum root mean square (RMS) value of residuals between the observed and calculated Curie point depths for all the numerical calculation patterns.

Results and discussion

Optimal model

In the numerical simulation, we calculated a combination of several unknown model parameters and determined the optimal model. The unknown parameters to be varied were (1) the effective friction coefficient, which influences the shear stress in Eqs. (8) and (9) and contributes to frictional heating in Eq. (7) at the plate interface; (2) the downdip limit of the high viscosity region, which was introduced by considering the possible existence of mega-intrusion rocks or partially serpentinized stagnant forearc mantle near the tip of the mantle wedge[6], or the nonuniform thickness of the continental crust, which is the thickest just beneath the TMVB and thins out towards the coast[29]; and (3) the viscosity of the high viscosity region. The effective friction coefficient (1) was systematically varied from 0.00425 to 0.02125 in small increments of 0.00425, the downdip limit of the highly viscous region (2) was varied from 35 to 60 km with an increment of 5 km, and the viscosity of the highly viscous region (3) was tested for six cases between 1.0×10^{23} Pa s and 1.0×10^{28} Pa s with an increment of 10 times. A total of 180 different combinations of the values of the unknown model parameters were tested numerically. In the optimal model, which minimizes the value of the RMS, the effective friction coefficient, downdip limit of the high viscosity region, and viscosity of the high viscosity region are 0.0085, 50 km, and 1.0×10^{25} Pa s, respectively. Fig. S6 shows the RMS value variations when one of these three optimal values is fixed and the remaining two parameters are varied. Figure 3 compares the observed Curie point depth distribution with the calculated distribution for the optimal model. As a contribution to the temperature field of the unknown parameters, frictional heating affects the subduction interface between the Cocos plate and the North American plate. Since the upper crust and lower crust were set with thicknesses of 16 km, respectively, changing the effective friction coefficient affected the temperature field near the plate interface up to a depth of 32 km (Fig. S6). The high viscosity region is more viscous than the surrounding mantle and therefore hampers the influx of hot mantle material into the mantle wedge corner. As a result, the higher the viscosity is, the more likely this region becomes stagnant and colder. In addition, the observation data of the Curie point depth distribution along the TMVB in the model region are particularly shallow, indicating a rather high vertical thermal gradient. This particular region was excluded when the RMS value was calculated because the convective heat source caused by volcanoes was not considered in our numerical model.

Thermal structure

Comparing the rupture area of past megathrust earthquakes with the interplate temperature for the optimal model, the temperature is estimated to range from 200 to 400 ℃, which is almost consistent with where the interplate slip mode has shown unstable sliding in previous studies[7,30,31]. On the other hand, in and around the Guerrero seismic gap, where the slab geometry is concave, the interplate temperature for the optimal model is estimated to be lower by approximately 100 ℃ than that in the neighbouring along-arc region at the same depths (Fig. S1). This suggests the formation of a region characterized by partial stick-slip behaviour.

On the other hand, the interplate temperature for an L-SSE occurrence region is estimated to range from 350 to 550 ℃ (Fig. 4a), except for the downdip side of the Guerrero seismic gap region. The upper limit temperature of 350 ℃ is consistent with the temperature at which the brittle-ductile transition takes place[7,29,30]. In the downdip side of the Guerrero seismic gap region, L-SSE occurrence region extends to the shallower depths at lower temperatures, but the updip limit temperature in the region with the largest slip (~ 14 cm) is estimated to be close to 350 ℃ (Fig. 4a). The average slip deficit in the Guerrero seismic gap has been reported to be small compared

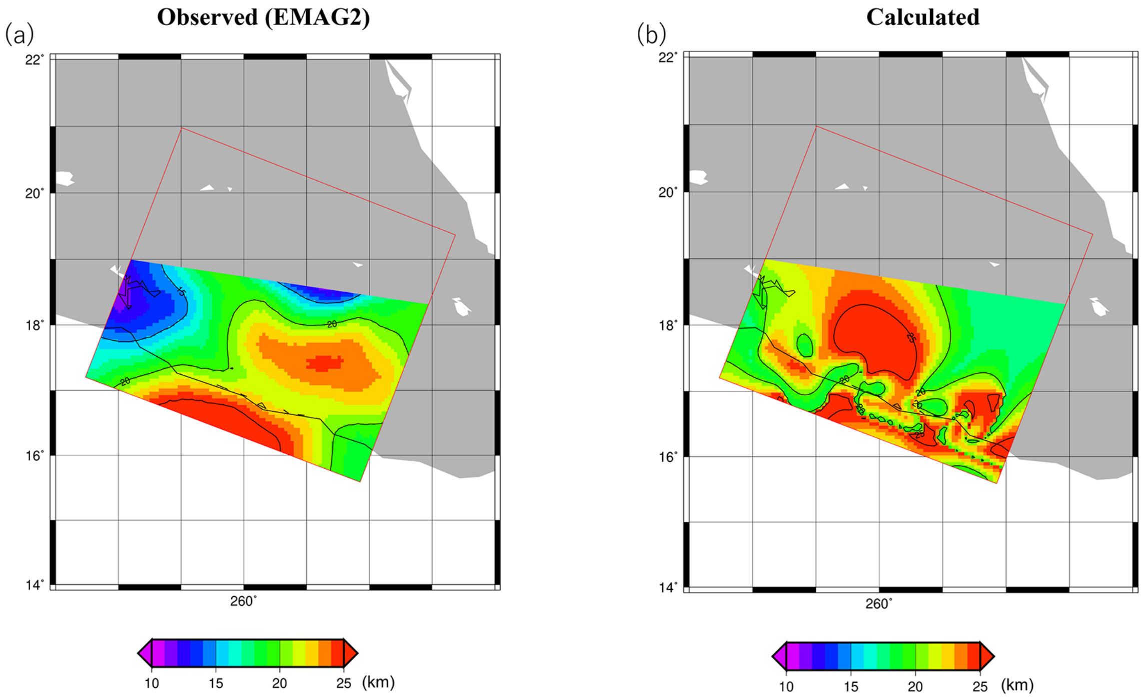

Fig. 3. Comparison of observed and calculated Curie point depth distributions. The calculated value is obtained from the best-fit model that has the minimum RMS value shown in Figure S4. The combination of unknown model parameters is as follows: effective friction coefficient of 0.0085, downdip limit of the high viscosity region on the plate interface of 50 km, and viscosity of 10^{25} Pa s. (a) Observed Curie point depth distributions. (b) Calculated Curie point depth distributions for the best-fit model. The map was created using GMT[41] (version 4.5.7, https://www.generic-mapping-tools.org/download/).

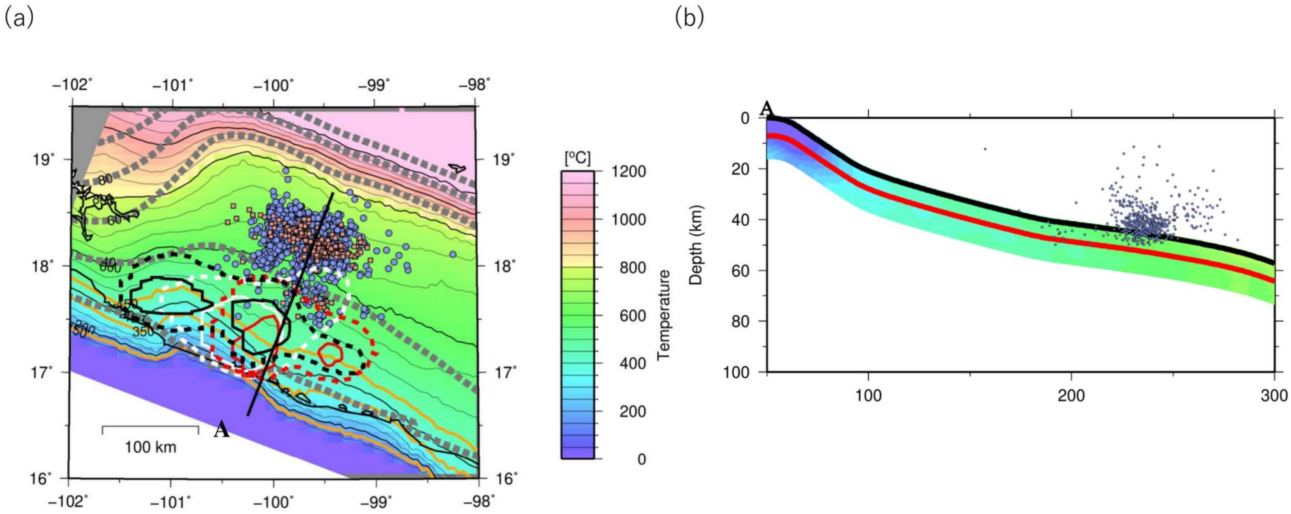

Fig. 4. (**a**) Calculated temperature at the upper surface of the Cocos plate for the best-fit model to the observed Curie point depth distribution, as viewed from the top. The grey dashed lines represent the isodepth contour lines of the upper surface of the subducted Cocos plate at 20-km intervals. The thin black solid lines represent the interplate temperature isotherms, and the orange solid lines emphasize the 150, 350, and 450 °C isotherms. The others are the same as those in Fig. 1. (**b**) Calculated temperature distributions on the vertical cross section along profile A in Fig. 4a. The black and red solid lines represent the slab surface and the bottom of the oceanic crust, respectively. The others are the same as those in Fig. 1. The map was created using GMT[41] (version 4.5.7, https://www.generic-mapping-tools.org/download/).

with the slip deficits on both sides of the seismic gap[18], suggesting that the Guerrero seismic gap region releases considerable strain energy through the occurrence of SSEs. Considering only the temperature constraints on the plate boundary, the mechanism by which L-SSE occurrence region extends to shallower depths in the Guerrero seismic gap region is unclear, but we consider this phenomenon later, as well as the dehydration process from the slab.

Furthermore, Fig. 4b shows the calculated temperature structure on the vertical cross section along the profile A in Fig. 4a passing through the region where the hypocentres of TTs are most concentrated. The temperatures for the occurrence of TTs range from 500 to 700 ℃ (Fig. 4a,b). In addition, there are seaside and inland swarms in the TTs, which align almost parallelly in the along-arc direction. From the tectonic tremor dataset of Idehara et al. (2014)[4], we extracted hypocentres with source durations of more than 25 s and residual errors of less than 0.75 s, and used only data with small hypocentre depth errors (Figs. 1, 4, 5, and 6). Both seaside swarms and inland swarms have hypocentres concentrated near the plate interface. The temperature of the seaside swarm on the plate interface ranges from 500 to 570 ℃. The temperatures are consistent with the temperature range for the globally observed episodic tremor and slip (ETS) of ~ 575 ℃, which is specific for young and warm subduction zones such as Cascadia[32]. On the other hand, the interplate temperature corresponding to the inland swarm ranges from 600 to 700 ℃, approximately 100 ℃ higher than the upper limit of the interplate temperature expected for the ETS zone, which is specific for young subduction zones.

Water content distributions and dehydration gradients near the slab surface

We calculated the water content distributions near the plate interface using the calculated thermal structure and phase diagrams of hydrous minerals for the oceanic crust and slab mantle, which were obtained from the Perple_X program[33] (Fig. S7a,b). In this study, the thickness of the oceanic crust was assumed to be 7 km vertically from the plate boundary, and MORB was assumed to be a hydrous mineral within the oceanic crust. Additionally, we considered the slab mantle in the deeper portion and assumed that the ultramafic rock is a hydrous mineral. We assumed a sharp dehydration transition when a certain mineral within the oceanic crust and the slab mantle transformed into other minerals, which are stable at higher p–T conditions.

Figure 5 shows the results of the water content distribution along the plate interface for the optimal model. We observed that near the updip limit of the L-SSEs, a phase transition from blueschist to amphibole of MORB is expected to take place (Fig. 5a). In defining the dehydration gradient, which is the spatial difference in water content per unit distance in the subduction direction (Fig. 6), a high dehydration gradient of approximately 0.08 wt%/km was estimated to be associated with the phase transition (Fig. 6a). In particular, in the downdip side of the Guerrero seismic gap region, the location where the high dehydration gradient is estimated is consistent with the location from the updip side of the L-SSE slip (~ 10 cm) to the location of the maximum slip (~ 14 cm) (Fig. 6a). On the other hand, in the region adjacent to the Guerrero seismic gap in the along-arc direction, the estimated dehydration gradient of MORB with the same L-SSE occurrence range is approximately 0.02 wt%/km (Fig. 6a). The amount of slip due to the L-SSE in the downdip side of the Guerrero gap area is estimated to be approximately 4 times greater than that in the adjacent area. Thus, it may be possible that the increase in pore pressure has reduced the effective normal stress, causing the slip to progress to shallower areas[34].

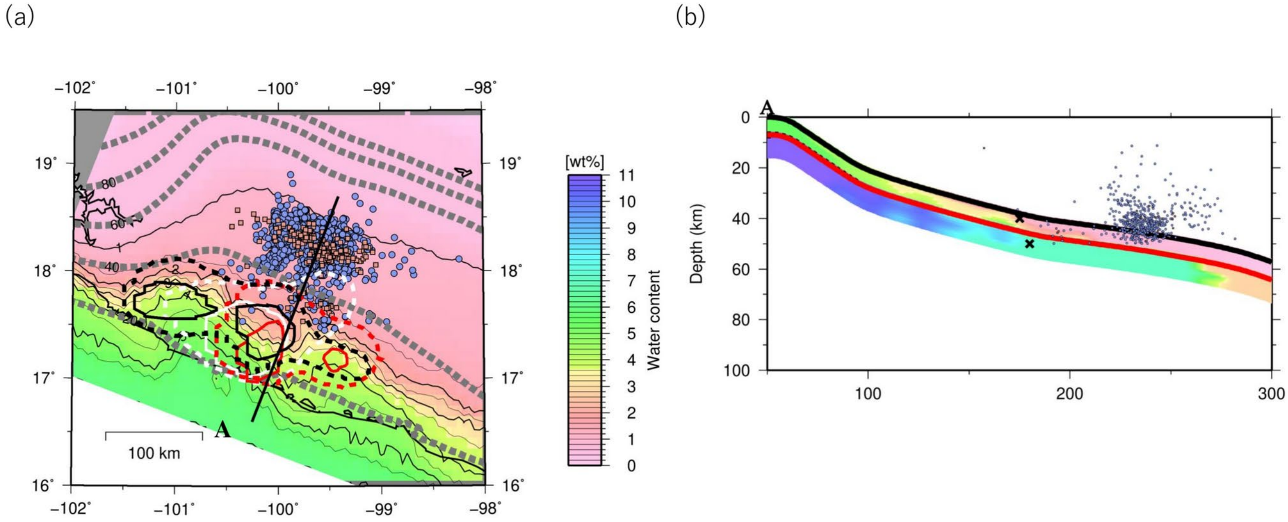

Fig. 5. (**a**) Calculated water content distribution at the upper surface of the Cocos plate for the best-fit model to the observed Curie point depth distribution, as viewed from the top. Thin black solid lines represent contours of the water content distribution at the plate interface. The others are the same as those in Fig. 4a. (**b**) Calculated water content distributions on the vertical cross section along profile A in (**a**). The others are the same as those in Fig. 4b. Black crosses show the approximate locations of phase transitions from amphibole to amphibole eclogite of MORB for the oceanic crust, and from brucite to antigorite of ultramafic rock for the oceanic lithosphere. The map was created by using the Generic Mapping Tools (GMT)[41] (version: 4.5.7, https://www.generic-mapping-tools.org/download/).

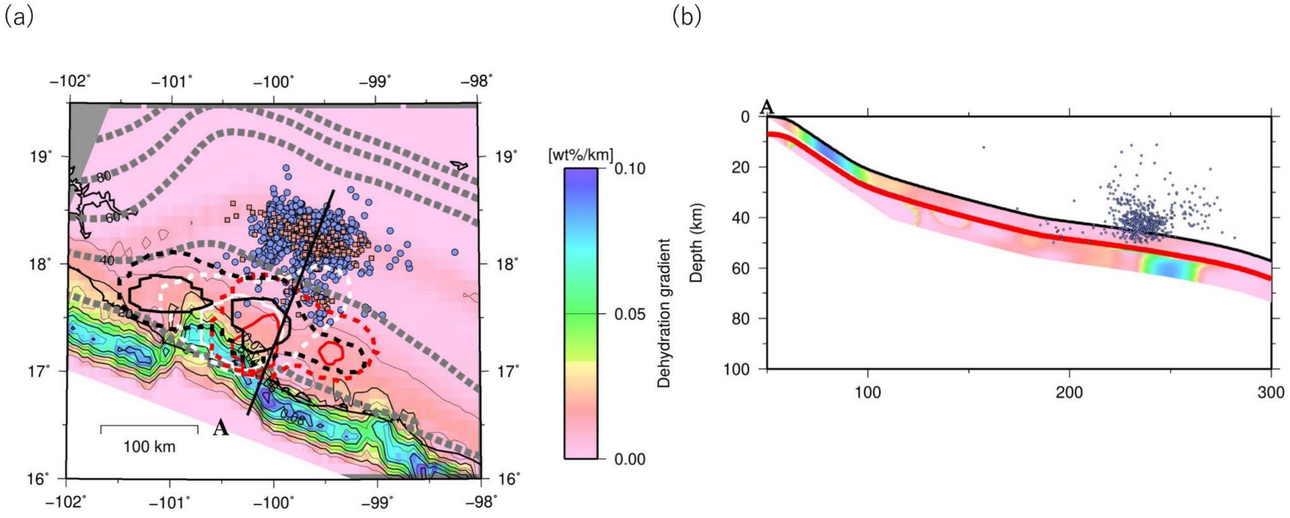

Fig. 6. (**a**) Calculated dehydration gradient at the upper surface of the Cocos plate for the best-fit model to the observed Curie point depth, as viewed from the top. Thin black solid lines represent contours of the dehydration gradient at the plate interface. The others are the same as those in Fig. 4a. (**b**) Calculated dehydration gradient distributions on the vertical cross section along profile A in (**a**). The others are the same as those in Fig. 4b. The map was created by using the Generic Mapping Tools (GMT)[41] (version: 4.5.7, https://www.generic-mapping-tools.org/download/).

On the other hand, in and around the seaside swarm of the TT, owing to the increased p–T conditions, phase transitions from amphibole to amphibole eclogite of MORB near the plate interface and from brucite to antigorite of ultramafic rock within the slab mantle are estimated (Fig. 5a,b). . In the inland swarm region, MORB has already undergone a phase transition to a hydrous mineral assemblage specific for amphibole eclogite or dry eclogite (Fig. 5a). Moreover, a phase transition from antigorite to chlorite in ultramafic rock is estimated just beneath it (Fig. 5b). The dehydration gradient was estimated to be approximately 0.01 wt%/km, associated with the phase transition from amphibole to amphibole eclogite near the seaside swarm. On the other hand, the dehydration gradients associated with the phase transitions from brucite to antigorite and from antigorite to chlorite in ultramafic rock are estimated to be approximately 0.02 and 0.06 wt/km near the seaside and inland swarms, respectively (Fig. 6a,b). Therefore, a larger dehydration gradient is estimated beneath the inland swarm, which has a greater number of TT hypocentres than the seaside swarm.

In conclusion, considerable dehydration from MORB and ultramafic rock takes place in the L-SSE occurrence region and inland swarm of TTs, respectively. A moderate dehydration front from ultramafic rock within the slab mantle was identified near the seaside swarm of TTs. Therefore, each dehydration process is considered to be related to the occurrence of slow earthquakes.

Conclusions

In this study, we performed 3-D thermomechanical subduction modelling around the Guerrero seismic gap region in Mexico to investigate the generation mechanisms of megathrust earthquakes, L-SSEs and TTs. Additionally, we examined the water content distributions and dehydration gradients near the slab surface associated with the subduction of the Cocos plate via phase diagrams of hydrous minerals within the slab. The significant results obtained in this study can be summarized as follows:

(1) The most suitable set of parameters for the effective friction coefficient, downdip limit of the high viscosity region, and viscosity within the high viscosity region that best explain the observed Curie point depth data are 0.0085, 50 km, and 1.0×10^{25} Pa s, respectively.
(2) These findings suggest that the interplate temperature in the Guerrero gap is lower than that in the adjacent area in the along-arc direction because a concave slab shape is present and that incomplete stick-slip behaviour occurs when the temperature is lower than the temperature at which smectite dehydrates. The interplate temperatures where megathrust earthquakes and L-SSEs occur range from 200 to 400 ℃ and 350 to 550 ℃, respectively, and those where seaside swarms and inland swarms of TTs occur range from 500 to 570 ℃ and 600 to 700 ℃ , respectively.
(3) Phase transitions with large dehydration gradients ranging from 0.01 wt% to 0.08 wt% were estimated to be derived from MORB within the oceanic crust and ultramafic rock within the slab mantle, indicating that the presence of dehydrated water near the plate interface is likely related to the occurrence of slow earthquakes.

Methods

In this study, we used an anelastic liquid approximation. As governing equations, we used mass conservation, momentum, and energy equations to calculate the temperature and flow fields. The mass conservation equation can be written as

$$\nabla \cdot [\rho_s(z)\mathrm{v}] = 0, \tag{2}$$

where z, $\rho_s(z)$ and $\mathbf{v}$ are vertical component in the Cartesian coordinate system, the fluid density and flow velocity vectors, respectively. The subscript denotes the adiabatic state. Following Yoshioka and Murakami (2007)[35], the momentum equation can be written as follows:

$$-\frac{\partial P}{\partial x_i} + \frac{\partial \tau_{ij}}{\partial x_j} + Ra\alpha(T - T_s)\delta_{i3} = 0, \tag{3}$$

where P is the pressure deviation from the hydrostatic pressure, τ_{ij} is a stress tensor, R_a is the Rayleigh number, α is the thermal expansivity, T is the temperature, and δ_{ij} is Kronecker's delta. T_s can be written as

$$\frac{dT_s}{dx_3} = Di_z T_{s.} \tag{4}$$

The dissipation number Di_z is given by

$$Di_z = \frac{g\alpha D}{C_p}, \tag{5}$$

where g is gravity acceleration, D is the thickness of the model, and C_p is the specific heat at constant pressure. The energy equation is expressed as

$$\rho c_p \left(\frac{\partial T}{\partial t} + \mathrm{v} \cdot \nabla T \right) = k\nabla^2 T + \eta(\nabla v)^2 + \rho g \alpha T v + H_r \rho + Q_f, \tag{6}$$

where t represents time, k represents thermal conductivity, v represents the vertical component of the flow velocity $\mathbf{v}$, H_r represents heat generation by a radioactive element, and Q_f represents frictional heating. The density ρ is dependent only on the temperature. Frictional heating Q_f[36] can be written as

$$Q_f = Min(\tau_b, \tau_d)\frac{v_t}{w}, \tag{7}$$

where τ_b and τ_d are the shear stresses at the plate boundary in the brittle and ductile regimes, respectively, v_t is the subduction velocity, and w is the thickness of the plate boundary deformation zone. The shear stress τ_b in the brittle regime[37] is written as

$$\tau_b = 0.85\sigma_n \left(1 - \lambda\right), \tag{8}$$

where σ_n is the normal stress and where λ is the pore pressure ratio.

The effective friction coefficient μ' is written as

$$\mu' = 0.85(1 - \lambda) \tag{9}$$

On the other hand, shear stress in the ductile regime[38] can be written as

$$\tau_d = \frac{1}{2} A^{-\frac{1}{n}} \varepsilon^{\bullet\frac{1}{n}} \exp\left(\frac{E'}{nRT}\right) \tag{10}$$

where A is a coefficient, $\dot{\varepsilon}$ is the shear strain rate, and E' is the activation energy.

Following Burkett and Billen (2010)[39], we use viscosity, which is represented by a composite of diffusion creep and dislocation creep:

$$\eta_{eff} = \frac{\eta_{dif}\eta_{dis}}{\eta_{dif} + \eta_{dis}}, \tag{11}$$

with

$$\eta_{dif,dis} = \left(\frac{d^p}{AC_{OH}^r}\right)^{\frac{1}{n}} \dot{\varepsilon}_{eff}^{\frac{1-n}{n}} \exp\left(\frac{E + P_{lc}V}{nRT}\right), \tag{12}$$

where η_{diff} and η_{disl} are the viscosities of diffusion and dislocation creeps, respectively, d is the grain size, p is the grain index, A is a coefficient, C_{OH} is the water content, r is the water content index, n is the stress index,

$\dot{\varepsilon}_{eff}$ is the second invariant of the strain rate tensor, E is the activation energy, P_{lc} is the lithostatic pressure defined by the depth gradient of compressibility, V is the activation volume, and R is the gas constant.

Data availability

The datasets generated and/or analysed during the current study are available in the dataset for the thermal convection model in Mexico at the uploaded URL (http://datadryad.org/stash/share/DQGSX1LR8nIzM4H7L4ReLBY0H2i7mm3yst5wfmFWn8I).

Received: 2 July 2023; Accepted: 19 February 2025

References

1. DeMets, C., Gordon, R. G. & Argus, D. F. Geologically current plate motions. *Geophys. J. Int.* **181**, 1–80 (2010).
2. Suarez, G. & Albini, P. Evidence for great tsunamigenic earthquakes (M 8.6) along the Mexican subduction zone. *Bull. Seismol. Soc. Am.* https://doi.org/10.1785/0120080201 (2009).
3. Radiguet, M. et al. Slow slip events and strain accumulation in the Guerrero gap, Mexico. *J. Geophys. Res. Solid Earth* https://doi.org/10.1029/2011JB008801 (2012).
4. Idehara, K., Yabe, S. & Ide, S. Regional and global variations in the temporal clustering of tectonic tremor activity. *Earth Planets Space* **66**(1), 1–10 (2014).
5. Payero, S. et al. Nonvolcanic tremor observed in the Mexican subduction zone. *Geophys. Res. Lett. Solid Earth* https://doi.org/10.1029/2007GL032877 (2008).
6. Jodicke, H. et al. Fluid release from the subducted Cocos plate and partial meltingof the crust deduced from magnetotelluric studies in southern Mexico: Implications for the generation of volcanism and subduction dynamics. *J. Geophys. Res.* **111**, B08102. https://doi.org/10.1029/2005JB003739 (2006).
7. Currie, C., Hyndman, R., Wang, K. & Kostoglodov, V. Thermal models of the Mexico subduction zone: Implications for the megathrust seismogenic zone. *J. Geophys. Res.* **107**(B12), 2370. https://doi.org/10.1029/2001JB000886 (2002).
8. Wada, I. & Wang, K. Common depth of slab-mante decoupling: Reconciling diversity and uniformity of subduction zones. *Geochem. Geophys. Geosys.* https://doi.org/10.1029/2009GC002570 (2009).
9. Manea, V. & Manea, M. Flat-slab thermal structure and evolution beneath central Mexico. *Pure Appl. Geophys.* **168**, 1475–1487 (2011).
10. Rosas, J. C., Currie, C. A., Harris, R. N. & He, J. Effect of hydrothermal circulation on slab dehydration for the subduction zone of Costa Rica and Nicaragua. *Phys. Earth Planet. Inter.* **255**, 66–79 (2016).
11. Li, C. F., Lu, Y. & Wang, J. A global reference model of Curie-point depths based on EMAG2. *Sci. Rep.* **7**(1), 1–94 (2017).
12. Ji, Y. & Yoshioka, S. Effects of slab geometry and obliquity on the interplate thermal regime associated with the subduction of three-dimensionally curved oceanic plates. *Geosci. Front.* **6**, 61–78 (2015).
13. Suenaga, N., Numerical modeling of temperature and flow fields associated with subduction of oceanic plates in central Japan and Mexico - considerations on the relationship between calculated temperature fields and occurrences of interplate earthquakes. https://hdl.handle.net/20.500.14094/D1006611. (2016).
14. McKenzie, D. Speculations on the consequences and causes of plate motions. *Geophys. J. Int.* **18**(1), 1–32. https://doi.org/10.1111/j.1365-246X.1969.tb00259.x (1969).
15. Grose, C. J. Properties of oceanic lithosphere: Revised plate cooling model predictions. *Earth Planet. Sci. Lett.* **333**, 250–264 (2012).
16. Amante, C., & Eakins, B. W., 2009. ETOPO1 arc-minute global relief model: procedures, data sources and analysis.
17. Kostoglodov, V., Bandy, W., Dominguez, J. & Mena, M. Gravity and seismicity over the Guerrero seismic gap, Mexico. *Geophys. Res. Lett.* **23**(23), 3385–3388 (1996).
18. Plata-Martínez, R. et al. Shallow slow earthquakes to decipher future catastrophic earthquakes in the Guerrero seismic gap. *Nat. Commun.* **12**(1), 3976 (2021).
19. Manea, V., Manea, M. & Ferrari, L. A geodynamical perspective on the subduction of Cocos and Rivera plates beneath Mexico and Central America. *Tectonophysics* **609**, 56–81 (2013).
20. Müller, R. D. et al. A global plate model including lithospheric deformation along major rifts and orogens since the Triassic. *Tectonics* **38**(6), 1884–1907 (2019).
21. Young, A. et al. Global kinematics of tectonic plates and subduction zones since the late Paleozoic Era. *Geosci. Front.* **10**(3), 989–1013 (2019).
22. Cao, X. et al. *A Deforming Plate Tectonic Model of the South China Block since the Jurassic* (Gondwana Research, 2020).
23. Villagómez, D. & Pindell, J. *Thermochronology of the Southern Mexican Margin (Xolapa Belt), Acapulco to Puerto Angel: Crustal Dynamics of a Trench-Trench-Transform Triple Junction* (Geological Society of America, 2021).
24. Schellart, W. P. Subduction dynamics and overriding plate deformation. *Earth Sci. Rev.* **253**, 104755 (2024).
25. Schellart, W. P., Stegman, D. R. & Freeman, J. Global trench migration velocities and slab migration induced upper mantle volume fluxes: Constraints to find an Earth reference frame based on minimizing viscous dissipation. *Earth Sci. Rev.* **88**(1–2), 118–144 (2008).
26. James, D. E., Fouch, M. J., Carlson, R. W. & Roth, J. B. Slab fragmentation, edge flow and the origin of the Yellowstone hotspot track. *Earth Planet. Sci. Lett.* **311**(1–2), 124–135 (2011).
27. Iwamoto, K. et al. 3-D thermal structure and dehydration near the Chile Triple Junction and its relation to slab window, tectonic tremors, and volcanoes. *Geosci. Lett.* **10**(1), 34 (2023).
28. Maus, S., Magnetic Anomaly Grid (2-arc-minute resolution). Version 2. NOAA National Centers for Environmental Information. https://doi.org/10.7289/V5MW2F2P. (2009).
29. Ferrari, L., Orozco-Esquivel, T., Manea, V. & Manea, M. The dynamic history of the Trans-Mexican Volcanic Belt and the Mexico subduction zone. *Tectonophysics* **522–523**, 122–149 (2011).
30. Hyndman, R., Wang, K. & Yamano, M. Thermal constraints on the seismogenic protion of the southwestern Japan subduction thrust. *J. Geophys. Res.* **100**, 15373–15392 (1995).
31. Hyndman, R., Yamano, M. & Oleskevich, D. A. The seismogenic zone of subduction thrust faults. *Island Arc* **6**(3), 244–260 (1997).
32. Peacock, S. M. Thermal and metamorphic environment of subduction zone episodic tremor and slip. *J. Geophys. Res. Solid Earth* https://doi.org/10.1029/2008JB005978 (2009).
33. Connolly, J. A. D. The geodynamic equation of state: what and how. *Geochem. Geophys. Geosys.* **10**, Q10014. https://doi.org/10.1029/2009GC002540 (2009).
34. Kita, S. et al. Effects of episodic slow slip on seismicity and stress near a subduction-zone megathrust. *Nat. Commun.* **12**(1), 7253 (2021).
35. Yoshioka, S. & Murakami, K. Temperature distribution of the upper surface of the subducted Philippine Sea plate along the Nankai Trough, southwest Japan, from a three-dimentional subduction model: relation to large interpolate and low-frequency earthquakes. *Geophys. J. Int.* **171**, 302–315 (2007).

36. Wang, K., Hyndman, R. D. & Yamano, M. Thermal regime of the Southwest Japan subduction zone: effects of age history of the subducting plate. *Tectonophysics* **248**(1–2), 53–69 (1995).
37. Byerlee, J. Friction of rocks. *Pure Appl. Geophys.* **116**(4–5), 615–626 (1978).
38. Caristan, Y. The transition from high temperature creep to fracture in maryland diabase. *J. Geophys. Res.* **87**, 6781–6790 (1982).
39. Burkett, E. R. & Billen, M. I. Three-dimensionality of slab detachment due to ridge-trench collision: Laterally simultaneous boudinage versus tear propagation. *Geochem. Geophys. Geosyst.* https://doi.org/10.1029/2010GC003286 (2010).
40. Tackley, P. J. & Xie, S. STAG3D: a code for modeling thermo-chemical multiphase convection in Earth's mantle. In *Computational Fluid and Solid Mechanics* (eds Tackley, P. J. & Xie, S.) (Elsevier Science Ltd, 2003).
41. Wessel, P. & Smith, W. H. F. New, improved version of the generic mapping tools released. *EOS Trans.* https://doi.org/10.1029/98EO00426 (1998).
42. Ahrens, J., Geveci, B. & Law, C. *ParaView: An End-User Tool for Large Data Visualization* (Elsevier, 2005).
43. Hayes, P. G. et al. Slab2, a comprehensive subduction zone geometry model. *Science* **362**, 58–61 (2018).
44. Kostoglodov, V. et al. A large silent earthquake in the Guerrero seismic gap, Mexico. *Geophys. Res. Lett.* https://doi.org/10.1029/2003GL017219 (2003).

Acknowledgements

We thank P. Tackley and K. Murakami for sharing the source codes of Stag3d by Tackley and Xie (2003)[40] and its improved version by Yoshioka and Murakami (2007)[35] for the thermomechanical computations. We also thank V. Kostoglodov and K. Kaneko for sharing slab geometry data around the Guerrero seismic gap and water content data of the oceanic crust and the mantle of the oceanic plate, using the Perple_X program, respectively. Figures were created by using the Generic Mapping Tools (GMT)[41] (version: GMT 4.5.7, URL link: https://www.generic-mapping-tools.org/download/), and the ParaView[42] (version: ParaView 5.4.1, URL link: https://www.paraview.org/download/). This work was partly supported by MEXT KAKENHI grant [grant numbers 21H05203] and Kobe University Strategic International Collaborative Research Grant (Type B Fostering Joint Research) and the UNAM-DGAPA-PAPIIT project grant IN114524.

Author contributions

N.S. carried out the computation for the 3-D thermomechanical subduction model and wrote the paper; S.Y. organized and instructed this study and edited the paper, V. C. M., M. M., and E. M. pointed out possible problems and advised the solutions to those in this study. Y.J improved the stag3D model used in this study so that it could be applied to subduction zones, and provided advice on how to handle the model. All authors reviewed and commented on the paper as well as declare no competing interests in relation to the work.

Declarations

Competing interests

The authors declare no competing interests.

Additional information

Supplementary Information The online version contains supplementary material available at https://doi.org/10.1038/s41598-025-91257-9.

Correspondence and requests for materials should be addressed to N.S.